JOURNAL OF PROPULSION AND POWER
Vol. 11, No. 2, March–April 1995

Dynamic Modeling of Starting Capabilities of Liquid Propellant Rocket Engines

T. J. Avampato* and C. Saltiel†
University of Florida, Gainesville, Florida 32611

An analytical technique is developed for predicting the mass flow rate and heat addition in a liquid propellant rocket engine fuel system during the initial portion of an engine start. The analysis emphasizes nozzle jacket heat exchange; specifically, flow and heat transfer characteristic influence on power availability. The outstanding feature of this model is the accurate representation of fluid properties during phase change, and the subsequent affect on mass flow rates. The model also considers conduction and energy storage within the nozzle walls and makes use of extensive hydrogen heat convection data. The analytical technique is applied to a proposed 20,000-lb thrust expander engine for the determination of the minimum initial nozzle jacket metal temperature that will promote starting at various operating conditions. The energy content of engine fuel flow during the initial portion of startup is compared to predicted turbomachinery torque requirements to determine start capability. Starting capability is determined for various initial nozzle metal temperatures at fuel inlet pressures of 50 and 70 psi at sea level. The minimum initial jacket metal temperature that will produce enough energy to overcome predicted turbine breakaway torque is determined to be 135°R for 70-psi and 385°R for 50-psi inlet pressures.

Nomenclature

A = passage area, in.^{2}
C_p = specific heat, Btu/lb/R
D = hydraulic diameter, ft
d = diameter, ft
d_t = turbine diameter, in.
f = friction factor
G = mass velocity, lb/ft^2/s
g_c = gravitational constant, ft/s^2
h = fluid enthalpy, Btu/lb
h_f = convective coefficient, Btu/in.^{2}/s/°R
h_{fg} = enthalpy change between saturated states, Btu/lb
k = thermal conductivity, Btu/ft/s/°R
l = length, ft
$\dot{m}$ = fluid mass flow rate, lb/s
Nu = Nusselt number
Pr = Prandtl number
p = fluid pressure, psi
Q = heat flux per unit length, Btu/s/ft
Re = Reynolds number
r = radial position, in.
S = suppression factor
stg = number of turbine stages
T = metal temperature, °R
Tq = turbine torque, ft-lb
t = time, s
u/c = turbine velocity ratio
V = fluid velocity, ft/s
X_{tt} = Martinelli parameter
x = fluid quality
α = thermal diffusivity, ft^2/s
Δh_i = ideal turbine enthalpy change, Btu/lb
ΔP = superheat pressure difference, psid
ΔT = total wall superheat, °R
η = turbine efficiency
θ = tangential position, rad
λ = fluid heat of vaporization, Btu/lb
μ = dynamic viscosity, lb/ft/h
ν = kinematic viscosity, ft^2/s
ρ = fluid density, lb/ft^3
ρ_h = fluid density gradient with respect to enthalpy
ρ_p = fluid density gradient with respect to pressure
σ = fluid surface tension, lb/ft

Subscripts
b = bulk
l = saturated liquid
r = radial direction
v = saturated vapor
w = wall
θ = tangential direction

Received Jan. 21, 1994; revision received July 5, 1994; accepted for publication Aug. 10, 1994.

*Graduate Student, Department of Mechanical Engineering; currently Pratt & Whitney Government Engine Business, West Palm Beach, FL.

†Assistant Professor, Department of Mechanical Engineering.

I. Introduction

THE prediction of the start characteristics of liquid propellant rocket engines is important to the engine configuration and control system design processes. Engine start systems receive secondary considerations since high-power performance is the chief design objective. Careful synchronization of control actions with transient start processes is required to deliver the smooth thrust buildup characteristics desired. The ability to power turbomachinery prior to combustion chamber ignition is an important design concern. Thrust buildup can be delayed or inhibited if turbine power is insufficient to accelerate propellant pumps. Many difficulties associated with engine start predictions stem from the nonlinear mass flow and heat transfer characteristics associated with filling unconditioned engine systems with cryogenic propellants. Fluid properties are strong functions of temperature and pressure, and high heat transfer rates result in abrupt changes in phase. Accurate predictions are especially important in engine cycles where this initial propellant flow provides all of the available turbine power for starting, e.g., expander cycles.

Expander cycle engines are power limited by heat transfer to the liquid fuel within the nozzle jacket. The starting power availability of these engines can be completely characterized by the fuel system heat transfer during the initial seconds of

start, and the engine pressure drop, which is given by the engine operating environment. All startup power is stored as potential energy in the form of latent heat in the fuel system and vehicle tank pressure head. Parametric studies, performed using an accurate startup prediction tool, can determine the starting envelope for expander engines.

The flow path of a typical expander cycle is shown in Fig. 1. At start, engine fuel, typically liquid hydrogen, flows from the propellant tank through the nonrotating pump, nozzle cooling jacket, and turbine, discharging to ambient via the nozzle. Turbine mass flow rate and enthalpy drop produce the necessary torque to power the propellant pumps. Heat addition to the fuel from the nozzle jacket walls directly influences turbine power by setting flow rate and turbine inlet temperature. A minimum temperature is required for starting if no additional mechanism is employed, e.g., an external spin assist. Clearly, an accurate assessment of the heat transfer characteristics of the nozzle jacket and fuel at this location is imperative. Heat transfer characterization of cryogenic fluids, such as liquid hydrogen, are extremely difficult since several convective heat transfer mechanisms are present simultaneously, e.g., film and nucleate boiling. Consideration of the complex heat transfer phenomena to the fluid make determination of the minimum initial nozzle jacket temperature necessary for engine start a difficult task.

Analysis of the starting process is given only a cursory treatment in liquid propellant rocket engine design books.[1,2] Most attempts to predict these processes and to design startup systems depend on experimental data for fine tuning prediction methods. Reference 3 describes test apparatus and analysis techniques for obtaining the start characteristics of engine components. The method requires the development of engine hardware and a dynamic analysis of data taken from low-range, high-response instrumentation during a simulated engine start. Hardware test methods are of little use in preliminary design, making more detailed analytical methods a necessity.

Analysis methods typically involve computer simulation using lumped parameter models of engine components.[4] Component characteristics are extrapolated from design conditions for use in startup predictions. Nozzle jacket heat transfer, however, cannot be adequately represented in this way. In particular, the variance in hydrogen properties from those at the design point require more than the simplistic representation typically used in these types of analysis.

An analytical technique is presented for determining the power available for startup of liquid fuel rocket engines by employing a detailed numerical model of heat transfer within the nozzle coolant jacket. The outstanding feature of this model is the accurate representation of fluid properties during phase change, and the subsequent affect on mass flow rates. The model also considers conduction and energy storage within the nozzle walls and makes use of extensive hydrogen heat convection data. This technique has been shown to match engine data taken during startup of a well-instrumented Space Shuttle Main Engine when measured jacket coolant inlet conditions are used as boundary conditions.[5] In this work the method is applied to a proposed 20,000-lb thrust expander engine for the determination of the minimum initial nozzle jacket wall temperature that will promote starting at various operating conditions. The energy content of engine fuel flow during the initial portion of startup is compared to predicted turbomachinery torque requirements to determine breakaway capability. Starting capability is determined for various initial nozzle metal temperatures and engine inlet pressures at sea level.

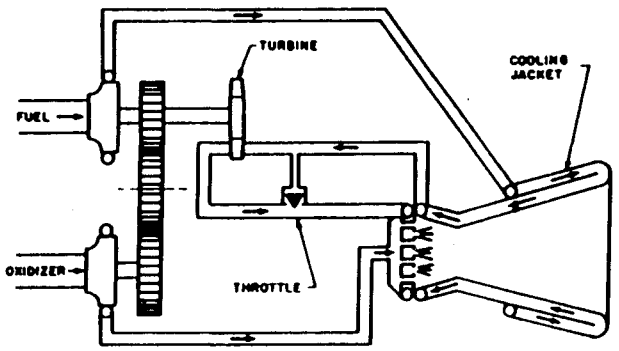

Fig. 1 Schematic of a typical expander cycle engine.

II. Analysis

Determination of the performance characteristics of the nozzle jacket heat exchanger requires the calculation of coolant mass flow and heat addition in the portion of the engine from the nozzle jacket coolant inlet manifold to the turbine inlet, as seen in Fig. 2. Liquid coolant enters the nozzle jacket from the inlet manifold and flows toward the nozzle throat cooling the jacket. The coolant is vaporized and exits the nozzle jacket as superheated or supercritical gas. The coolant undergoes a phase change and sudden expansion through the jacket as the unconditioned jacket metal temperature decreases. Heat addition comes initially from removing latent heat from the fuel system, until main chamber ignition, at which time heat addition is from combustion products expanding through the nozzle.

Coolant flow characteristics are calculated as a one-dimensional compressible flow with friction and heat addition. The continuity, momentum, and energy equations are combined and written to allow calculation of the pressure and enthalpy gradient along the flow path. The relations contain geometry, heat addition, friction, and fluid property terms. The jacket fluid inlet and discharge pressure and inlet enthalpy provide the boundary conditions for the analysis.

A. Coolant Mass Flow Rate Calculation

The derivation of local pressure and enthalpy changes along the flow path is analogous to the influence coefficient formulation for ideal gases found in Ref. 6. Using the chain rule to describe the functional relation of density on pressure and enthalpy in the flow direction x

$$\frac{\partial \rho}{\partial x} = \left.\frac{\partial \rho}{\partial h}\right|_{p} \frac{\mathrm{d}h}{\mathrm{d}x} + \left.\frac{\partial \rho}{\partial p}\right|_{h} \frac{\mathrm{d}p}{\mathrm{d}x} \tag{1}$$

pressure and enthalpy changes can be expressed as

$$\frac{\mathrm{d}p}{\mathrm{d}x} = \frac{\frac{1}{A}\frac{\mathrm{d}A}{\mathrm{d}x} - \left(1 - \frac{\rho_h V^2}{\rho g_c}\right)\frac{2f}{D} + \frac{\rho_h}{\rho}\frac{Q}{\dot{m}}}{-\frac{\rho_h}{\rho} + \frac{g_c}{\rho V^2} - \frac{\rho_h}{\rho^2}} \tag{2}$$

$$\frac{\mathrm{d}h}{\mathrm{d}x} = \frac{\frac{1}{\rho A}\frac{\mathrm{d}A}{\mathrm{d}x} - \frac{\rho_p V^2}{\rho g_c}\frac{2f}{D} + \left(\frac{\rho_p}{\rho} - \frac{g_c}{\rho V^2}\right)\frac{Q}{\dot{m}}}{-\frac{\rho_h}{\rho} + \frac{g_c}{\rho V^2} - \frac{\rho_h}{\rho^2}} \tag{3}$$

Time-dependent mass and energy terms are accounted for in the energy and continuity balances performed over each time interval. Note the similarity between Eqs. (2) and (3). A flow path area term, a heat addition term, and a wall friction term appear in the numerator. The area derivative is dictated by engine geometry. Q is determined via calculation of the heat conduction within the tube walls. The change in magnitude of ρ_h and ρ_p during phase change represents the nonlinear characteristics of the cooling process.

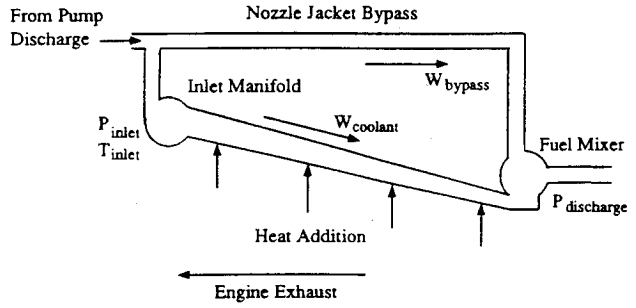

Fig. 2 Schematic of the nozzle jacket portion of an engine fuel system.

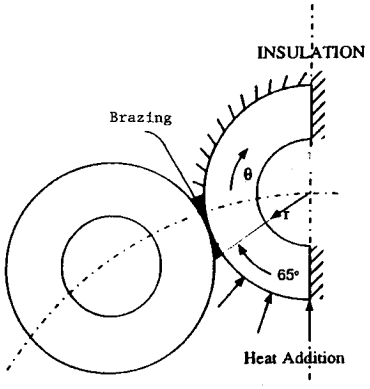

Fig. 3 Cross section of jacket coolant tubes, illustrating heat transfer boundary conditions.

B. Heat Transfer Calculation

Heat transfer in the jacket tube is described by a second-order partial differential equation for the local temperature

$$\frac{1}{r}\frac{\partial}{\partial r}\left(r\frac{\partial T}{\partial r}\right) + \frac{1}{r^2}\frac{\partial^2 T}{\partial \theta^2} = \frac{1}{\alpha}\frac{\partial T}{\partial t} \tag{4}$$

Heat along the i.d. is removed through forced convection to the hydrogen coolant. Figure 3 shows a section of the jacket tube illustrating the heat transfer boundary conditions. The tangential dependence is the result of the tangentially varying boundary condition and nonuniform heating on the tube o.d. Axial heat conduction is neglected. The contribution of axial conduction is small relative to the other components because of the small temperature gradient along the jacket length and the small cross-sectional area for conduction. The outer surface of the nozzle jacket tube receives a time-dependent temperature boundary condition on the hot gas side and an insulated boundary condition along the remaining circumference. Metal brazing connecting adjacent tubes allows only 130 deg of the tube o.d. to be exposed directly to hot gas. Insulation is formed over the exterior of the nozzle producing an insulated boundary condition on the portion of the tube o.d. opposite of the hot gas side. The portion of the tube o.d. adjacent to other tubes can be treated as an insulated boundary because of the tangential symmetry around the nozzle circumference, i.e., no temperature gradient from tube-to-tube. Because of this symmetry it is possible to perform calculations for only one-half of the tube.

The i.d. convective boundary condition is governed by several heat transfer mechanisms. Forced convection, nucleate boiling, and film boiling conditions can exist within the jacket nozzle. The coolant state, velocity, and tube wall temperature to fluid bulk temperature difference define the applicable convective heat transfer mechanism. Two-phase or subcooled hydrogen may undergo nucleate or film boiling. For superheated and supercritical states the heat flux is governed by single-phase forced convection. Empirical corrections are applied to analytical predictions for the various heat transfer regimes.

When subcooled or two-phase coolant is present in a tube section with a wall temperature greater than the tube saturation temperature, a boiling mechanism may contribute to the heat flux. Nucleate boiling heat transfer is calculated by superimposing the forced convection and boiling contributions to the heat transfer coefficient. When wall temperatures are significantly higher than the fluid saturation condition, a maximum or critical heat flux may be reached. This condition corresponds to the departure from nucleate boiling, at which point the heat flux drops significantly.

The forced convection heat transfer to subcritical fluids is governed by a modified form of the Dittus-Boelter relation.[7] For small wall to bulk temperature differences the heat transfer is governed completely by

$$Nu = 0.023Re^{0.8}Pr^{0.4}F \tag{5}$$

Nu, Re, and Pr are functions of the coolant velocity and flow properties. The Reynolds number factor F is an empirical correction calculated as a function of X_{tt}

$$X_{tt} = \left(\frac{1-x}{x}\right)\left(\frac{\rho_{\text{film}}}{\rho_l}\right)^{0.9}\left(\frac{\mu_l}{\mu_v}\right)^{0.1} \tag{6}$$

which is a measure of the fluid thermodynamic state. It is a function of the ratio of ρ at film and liquid conditions, the viscosity ratio at the saturated liquid and vapor conditions, and x. F is the ratio of the Reynolds number calculated at fluid bulk conditions to that calculated at saturated liquid conditions to the 0.8 power:

$$F = (Re/Re_l)^{0.8} \tag{7}$$

The dependence on the fluid quality is evident by the ability to represent F empirically as a function of the Martinelli parameter.[7] The Reynolds number factor goes to unity for saturated, subcooled, and superheated fluids.

In the two-phase and subcooled regions, when wall temperatures are greater than the fluid saturation temperature, a boiling mechanism is added to estimate the total heat transfer. Estimation of this boiling component is based on nucleate pool boiling relations with compensation made for fluid velocity. The heat transfer relations resulting from the coolant phase change is given in Ref. 7, where an empirical relation for the convective heat transfer coefficient is given as

$$h_{f-\text{boiling}} = 0.00122\left(\frac{k_l^{0.79}C_{pl}^{0.45}\rho_l^{0.49}g_c^{0.25}}{\sigma^{0.5}\mu_l^{0.29}\lambda^{0.24}\rho_v^{0.24}}\right)\Delta T^{0.24}\Delta P^{0.75}S \tag{8}$$

The fluid properties that govern pool boiling relations appear in Eq. (8). These properties, taken at their saturated liquid or vapor states, are k, C_p, ρ, σ, μ, and λ. Wall superheat is accounted for by ΔT, ΔP, and S.

The analysis of Ref. 8 developed the Nusselt number for pool boiling using a liquid Prandtl number and bulk Reynolds number. The bulk Reynolds number is governed by the bubble growth rate, which can be described by the effective, or mean, superheat across the boundary layer ΔT. For pool boiling the difference between the effective superheat and total wall superheat is negligible, however, this is not the case for convective nucleate boiling because of the fluid velocity's effect on the steepness of the temperature boundary layer.

Equation (8) uses the pool boiling relation with ΔT and S, to estimate the effective wall superheat. ΔP is the difference in the saturated pressures corresponding to ΔT. When wall temperatures are not greater than the fluid saturation temperature, there is no superheat, and no phase change contri-

bution to heat flux. The suppression factor is defined experimentally as a function of the liquid Reynolds number and X_{tt}. The suppression factor approaches unity at zero flow conditions and zero at infinite flow rate.

Convective heat flux increases as the wall to fluid bulk temperature difference increases until a maximum heat flux is reached, beyond which there is a dramatic decrease in heat flux. This critical heat flux marks the departure from nucleate boiling and the onset of film boiling. In film boiling a vapor region forms in an annulus adjacent to the heated tube wall. Heat convection characteristics approach those of forced gaseous convection as the energy removed by fluid phase change becomes limited by fluid interactions at the liquid/vapor boundary.

Determination of the critical heat flux follows,[9] which is valid for large length-to-diameter l/d ratio vertically heated tubes. The critical heat flux is related to the exit quality of the coolant; usually greater than zero for large l/d tubes. Critical heat flux is described using correlations based on coolant quality and a dimensionless mass flux parameter. The following relations are shown to match data for various regimes of the mass flux parameter[9]:

$$Q_{\text{crit}} = 1570.5Gh_{fg}\left(\frac{\rho_v}{\rho_l}\right)^{0.133}\left(\frac{\sigma\rho_l}{G^2l}\right)^{0.333}\left\{\frac{1}{[1 + 0.0031(l/d)]}\right\} \tag{9}$$

$$Q_{\text{crit}} = 5339.8Gh_{fg}\left(\frac{\sigma\rho_l}{G^2l}\right)^{0.043}\frac{d}{l} \tag{10}$$

$$Q_{\text{crit}} = 1539.1Gh_{fg}\left(\frac{\rho_v}{\rho_l}\right)^{0.133}\left(\frac{\sigma\rho_l}{G^2l}\right)^{0.433}\left\{\frac{(l/d)^{0.27}}{[1 + 0.0031(l/d)]}\right\} \tag{11}$$

The broad range of flow conditions studied requires the use of these slightly different correlations to produce a good match to the data. As a conservative estimate, in our studies we choose the lowest value of Q_{crit} from Eqs. (9–11). The wall to fluid bulk temperature difference corresponding to this heat flux determines whether nucleate or film boiling conditions exist in the nozzle jacket.

Film boiling is the process in which a vapor film forms in an annulus adjacent to the heated surface and liquid coolant flows through the center. Subcooled and saturated coolant can experience film boiling. Supercritical fluids exhibit film boiling characteristics analogous to subcritical fluids. Reference 10 is an extensive source of hydrogen film boiling data taken over a wide range of fluid velocity, wall temperature, and tube diameter. The film boiling convective heat transfer coefficient is calculated as a function of fluid Reynolds number, Prandtl number, and fluid state. The Martinelli parameter is used to apply empirical correction to a theoretical definition of the Nusselt number.

For subcritical hydrogen the coolant Nusselt number is given in Ref. 10 as

$$Nu = Nu_{\text{film}}\left\{\left[\frac{1}{(0.81 + 2.52X_{tt})}\right] + 0.12\right\} \tag{12}$$

The theoretical Nusselt number Nu_{film} is calculated using the Reynolds number and Prandtl number defined using properties taken at fluid film conditions

$$Nu_{\text{film}} = 0.021Re_{\text{film}}^{0.8}Pr_{\text{film}}^{0.4} \tag{13}$$

Again, the empirical correction is applied as a function of X_{tt}, given by Eq. (6).

Several correlations are given in Ref. 10 for the supercritical film boiling convective heat transfer coefficient. The correlation selected gives the most accurate results for tube diameters similar to those of the nozzle jacket tubes. The heat transfer coefficient, defined by a Martinelli parameter-based correction to the film Nusselt number, represents the best choice for this situation. The Martinelli parameter for supercritical hydrogen is defined using a pseudoquality.

The analysis treats supercritical fluid under film boiling conditions as consisting of low- and high-density regions. These are analogous to the subcritical film boiling vapor and liquid regions. The Martinelli parameter correction is given as a curve fit of empirical data $f(X_{tt})$, accounting for the fluid properties of the light and heavy regions. The form of this correlation is

$$Nu = Nu_{\text{film}}[1.0 + 0.01457(\mu_w/\mu_b)]f(X_{tt}) \tag{14}$$

where $f(X_{tt})$ is defined in Ref. 10.

At pressures above 800 psi the hydrogen convective heat transfer coefficient is defined by forced convection. Heat transfer experiments in Ref. 11 have determined that supercritical heat convection can be described by the Nusselt number relation

$$Nu = 0.021Re^{0.8}Pr^{0.4} \tag{15}$$

Since fluid state is well above the critical pressure, the two-phase film boiling phenomena no longer influences heat convection.

C. Fluid Properties and Process Interactions

The thermodynamic properties of the coolant have a strong influence on the flow rate and heat transfer characteristics in the jacket. In addition, the fluid expansion and heat transfer determine the fluid properties at locations along the flow path. The interactions of the heat transfer and coolant flow processes become evident upon examination of the governing equations. Depending on the coolant phase, mass flow rate and pressure drop relationships are significantly different. Fluid properties greatly effect heat transfer rates through their influence on the convective heat transfer coefficient. The relationships between pressure, density, and enthalpy also vary for different fluid states. This effects the governing equations in the form of the density derivative terms.

Vaporization of the coolant greatly reduces the mass flow rate, as the low density and small cross-sectional area at the end of the jacket passage set the flow rate. Heat addition is the main contributor to this phase change. Expanding coolant accelerates through the tube. The increased flow velocity results in an increase in the frictional pressure loss term of Eq. (2). The heat flux term in Eq. (2) accounts for the pressure loss associated with heat addition. Fluid density also effects the pressure loss relation. Higher fluid densities decrease the effect of friction and heat addition on pressure loss.

Heat addition, as expected, increases the enthalpy gradient along the passage defined by Eq. (3). The enthalpy gradient also is affected by the fluid velocity and friction losses. The heat addition and friction terms of Eqs. (2) and (3) are also strongly influenced by the fluid density and density derivatives.

The fluid temperature, velocity, and density greatly effect the heat transfer characteristics. The convective heat transfer coefficients for all regimes of convection are defined by the fluid Reynolds and Prandtl numbers. The convective heat transfer coefficient increases for high-velocity and high-density coolant flows. The fluid state also determines the applicable heat transfer mechanisms, i.e., film boiling or nucleate boiling. The dependence of all of these quantities on the relations of Eqs. (2) and (3) is the basis of the heat transfer and fluid dynamic process interactions.

The fluid density derivatives determine the extent to which heat addition and frictional losses effect the coolant pressure

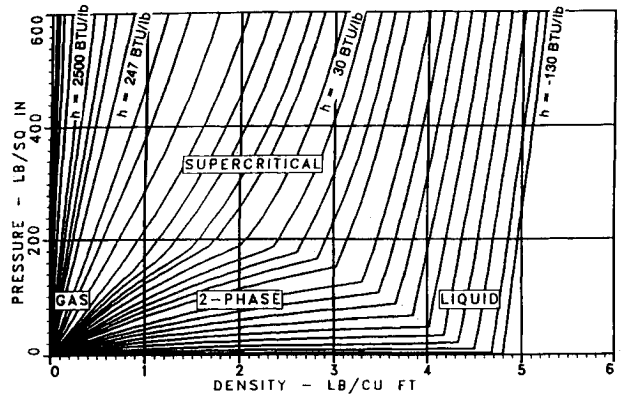

Fig. 4 Thermodynamic property map for hydrogen.

and enthalpy. The density derivatives ρ_h and ρ_p represent the change in density with respect to enthalpy and pressure, respectively. Figure 4 is a density/enthalpy/pressure map for hydrogen. Note the steepness of the density gradient with respect to pressure for gaseous states relative to that for liquids. The density derivative is positive in both cases. The density derivative with respect to enthalpy exhibits the opposite characteristic. Its value is larger for liquids than for gases and is negative for both liquids and gases. The friction and heat addition terms in the pressure loss relation [Eq. (2)], include the density/enthalpy relation. The density/pressure relation appears in the numerator of the enthalpy relation [Eq. (3)]. These quantities account for the density change as a result of physical processes acting on the fluid.

III. Numerical Approach

To accurately capture the performance characteristics of an engine at startup, a detailed simulation of the fluid and heat transfer processes within the nozzle jacket is required. The nonlinearities due to phase change in the flow make numerical solution of this conjugate problem computationally challenging. To simplify the analysis, calculation in the wall and flow regimes is solved independently at each time step.

The jacket flow path is discretized into a series of volume elements. The fluid property relations [Eqs. (2) and (3)] are integrated using rectangular numerical integration to calculate the pressure drop and property information along the passage length. The tube inlet flow rate is adjusted until the calculated pressure drop equals that given by boundary conditions. A secant-tangent iteration technique with bracketing is used.[12] Energy and continuity balances for each fluid volume are performed simultaneously via a nested iteration using the same numerical technique. Figure 5 illustrates the numerical approach to solving the governing equations. Grid density, time step, and convergence criteria are chosen conservatively so as to insure stability and accuracy. To obtain grid and temporal discretization independence of the solution, uniform grids of approximately 0.35 points/in. and a time step of 1×10^{-3} s were found sufficient. The convergence criteria were established as $\pm 0.005\%$ for both the fluid and energy calculations. Typically, up to 10 iterations on the outer loop are required to achieve convergence when two-phase flow is present.

The two-dimensional heat conduction equation in cylindrical coordinates is solved in "slices" of the nozzle jacket cross section corresponding to each fluid volume. A thermal resistance model is used to create a set of equations representing an energy balance in metal volume elements. Thermal resistances are calculated for internal metal elements and the jacket boundaries. The set of equations is solved simultaneously for the temperature distribution as a function of radial and tangential position. The matrix containing thermal resistances and a vector containing the current temperatures are

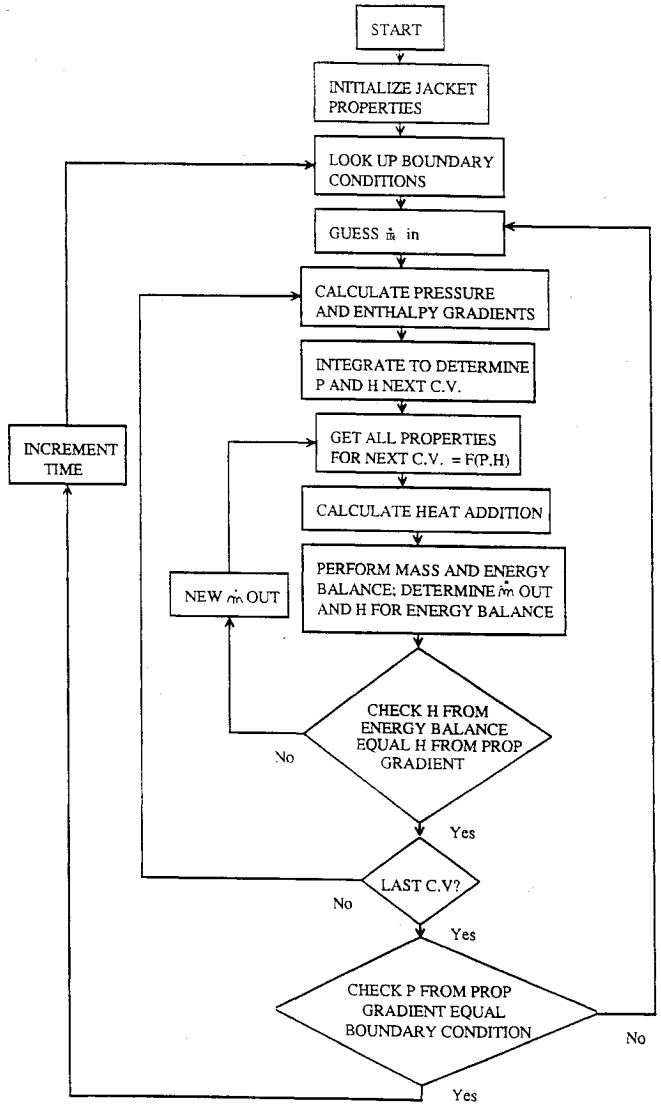

Fig. 5 Flow diagram illustrating the computational procedure.

solved for the new temperature at each location throughout the jacket. As in the fluid regime, grid density is chosen sufficiently fine to insure spatial discretization independence: 10 axial, 3 radial, and 12 tangential evenly spaced points were employed.

IV. Expander Cycle Engine Starting Capability Study

In an expander cycle all turbine power comes from heat addition to the hydrogen coolant. There is no combustion process upstream of the turbines. The analysis emphasizes the performance of the nozzle jacket heat exchanger, where heat transfer contributes greatly to turbine power availability. Jacket discharge flow rate must power engine turbomachinery sufficiently to allow rotation and engine acceleration. The nozzle-jacket analysis is coupled with a simplified engine model, including turbine performance and power calculations. Fuel pump pressure losses and heat transfer in the jacket supply line are considered negligible. Calculations are performed over the first $\frac{1}{4}$ s of the engine start, the time period in which turbine rotation must occur. Jacket fluid inlet and discharge pressure, inlet enthalpy, and jacket metal temperature provide the boundary conditions for the analysis. Jacket inlet pressure and enthalpy remain at propellant tank conditions, and metal temperatures cool only slightly from their initial condition during the short period of interest. Metal temperature effects on the nozzle jacket flow characteristics are de-

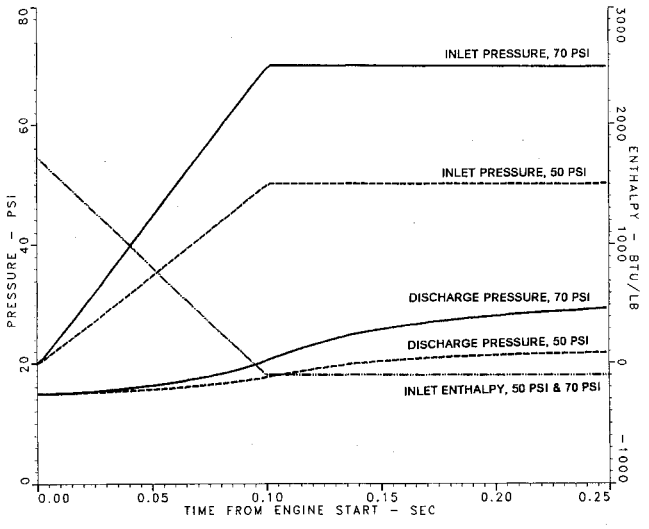

Fig. 6 Nozzle jacket boundary conditions for 50- and 70-psi fuel inlet pressures, and 520°R initial metal temperature.

termined, establishing a minimum metal temperature that will not promote turbine breakaway.

The nozzle jacket of this engine is constructed of 185 stainless steel tubes, 32.75 in. in length. The coolant passage forms the combustion chamber and nozzle, providing cooling of both hot gas systems. Hydrogen makes one pass through the jacket from the injector face, along the combustion chamber to the throat, and discharges at the nozzle exit plane. The tube diameter decreases to the throat and then increases as nozzle diameter increases, forming the divergent section. This produces a convergent-divergent flow path within the passage ranging in diameter from 0.07, to 0.03, to 0.13 in. at the inlet, throat, and discharge, respectively. Table 1 lists the nozzle properties.

Table 1 Nozzle properties

Jacket length	32.75 in.
Distance to throat	11.5 in.
Metal conductivity	2.176×10^{-4} Btu/in.^{2}/s/°R
Metal specific heat	0.1099 Btu/lb/°R
Metal density	0.2951 lb/in.^{3}

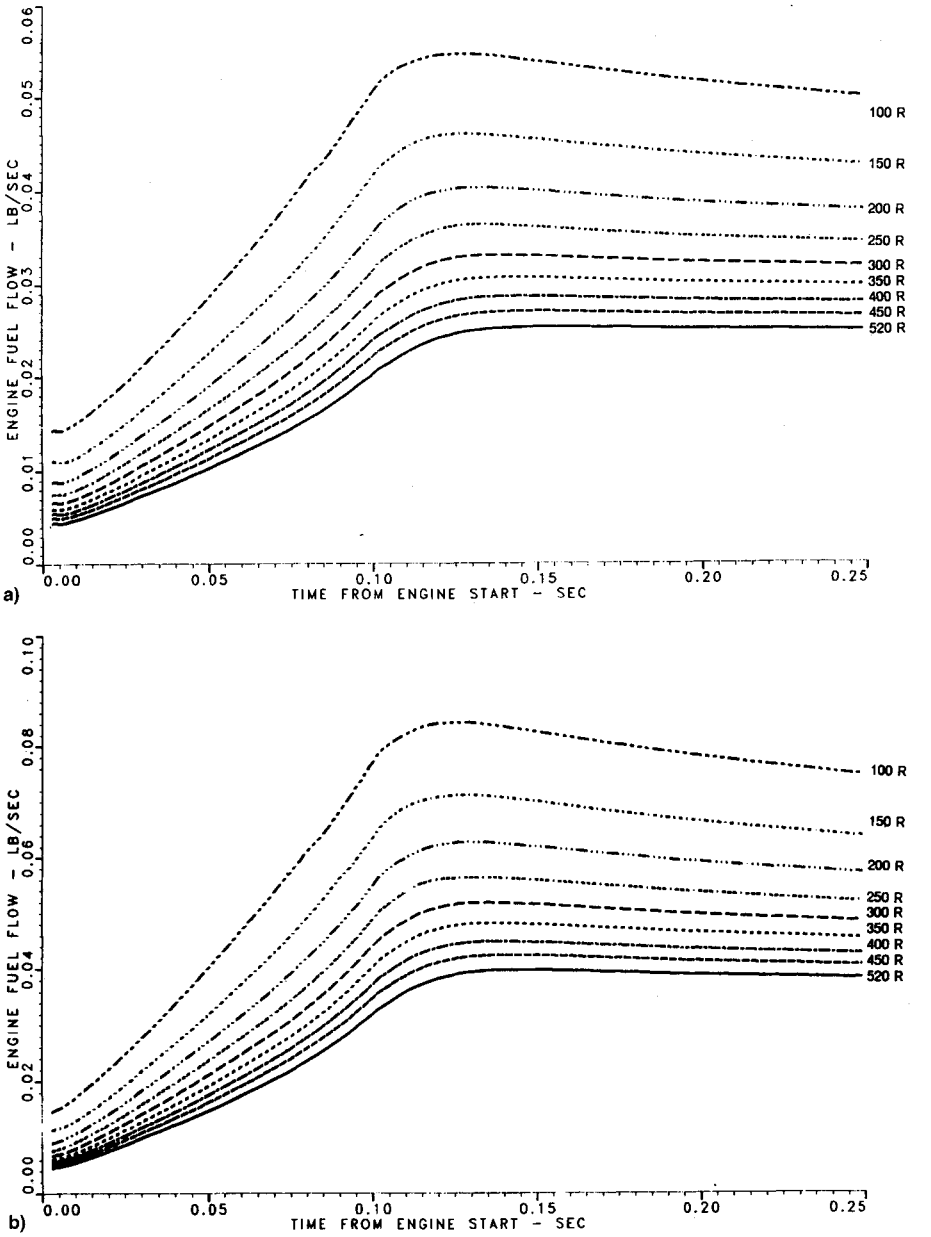

Fig. 7 Nozzle jacket hydrogen mass flow rate for various initial metal temperature at a) 50- and b) 70-psi fuel inlet pressures.

Hydrogen enters the nozzle jacket from the chilled-down pump upon sequencing of pump cooldown overboard and main fuel shutoff control valves. Nozzle jacket discharge flows through the nonrotating turbine and the combustion chamber injector to ambient pressure. The analysis is performed for a sea level start, where injector discharge is at atmospheric pressure. Simulations are performed for two engine fuel inlet pressures, 50 and 70 psi.

V. Discussion of Results

Jacket mass flow rate, heat addition, and turbine torque are calculated for start transients for engines with varying initial jacket metal temperatures. Engine fuel system, turbine, and injector calculations must be performed in conjunction with the nozzle jacket analysis. Turbine performance is documented in Ref. 13. Jacket discharge mass flow rate and enthalpy are used to calculate turbine torque. The predicted breakaway torque for this turbine is 0.6 ft-lb. If this torque is not achieved at any point during start there will be no turbopump rotation, and, consequently, no possibility of thrust buildup.

Figure 6 shows the jacket inlet and discharge pressure and inlet enthalpy boundary conditions used in the analysis for the 520°R metal temperature. Pressure and enthalpy are ramped to engine inlet conditions in 0.1 s, representing the response characteristic of typical engine control valves. Jacket discharge pressure is set by the turbine and injector flow characteristics.

Figure 7 shows the calculated total jacket hydrogen mass flow rate for all tubes during the first 0.25 s of engine starts with initial metal temperatures ranging from 520 to 100°R. Mass flow rate increases from 0 to 0.1 s as inlet pressure increases. Flow rates peak just after 0.1 s and then decrease slightly as the jacket is back-pressured by increasing injector flow. Colder metal temperatures produce higher mass flow rates. The decreased heat transfer results in higher density fluid throughout the jacket and higher mass flow rates. At the steady-state conditions reached by 0.25 s, mass flow ranges from 0.04 to 0.077 lb/s for an inlet pressure of 70 psi, and from 0.025 lb/s to 0.050 lb/s at 50 psi as initial metal temperature is decreased from 520 to 100°R.

Hydrogen exiting the nozzle jacket has been heated to a temperature equal to the metal temperature at the jacket discharge. Jacket metal cooling begins at the inlet of the passage, progressing toward the discharge as colder fluid begins to fill the jacket. Over the short duration of interest, little heat is removed from the discharge end of the jacket. Coolant discharge enthalpy is set by the metal temperature and fluid pressure at the jacket discharge. The peak discharge enthalpy over the 0.25-s transient ranges from 1730 to 250 Btu/lb for 70-psi inlet pressure, and from 1730 to 245 Btu/lb for 50 psi.

The fluid temperature change along the jacket length produces variable heat transfer conditions within the passage. Figure 8 shows the longitudinal fluid and wall temperature gradients for the near steady conditions at 0.25 s for the 70-psi inlet pressure, 520°R temperature case. Boiling begins almost immediately upon entering the jacket passage since the jacket temperature is much greater than the hydrogen saturation temperature. Since the wall to fluid temperature difference, corresponding to the departure from nucleate boiling, is less than 10°R, film boiling conditions exist in this region. The saturated vapor condition, at which point the fluid becomes a single-phase vapor, is clearly marked on the figure. Downstream of this point, heat transfer is characterized by single-phase forced convection. As the coolant temperature approaches the jacket temperature further downstream, heat transfer diminishes.

Turbine torque at 0 rpm is calculated using nozzle jacket discharge flow rate, and enthalpy

$$T_q = 0.145\dot{m}d_t[\Delta\eta/\Delta(u/c)]\sqrt{stg}\sqrt{\Delta h_i} \qquad (16)$$

where $\Delta\eta/\Delta(u/c)$ is the slope of the efficiency vs tip velocity ratio. The slope of the efficiency vs tip velocity ratio is ob-

Table 2 Turbine and injector characteristics

Turbine area	0.29 in.^{2}
Turbine diameter	6.75 in.
$[\eta/(\Delta u/c)]$	3.9
Turbine stages	1
Injector area	0.218 in.^{2}

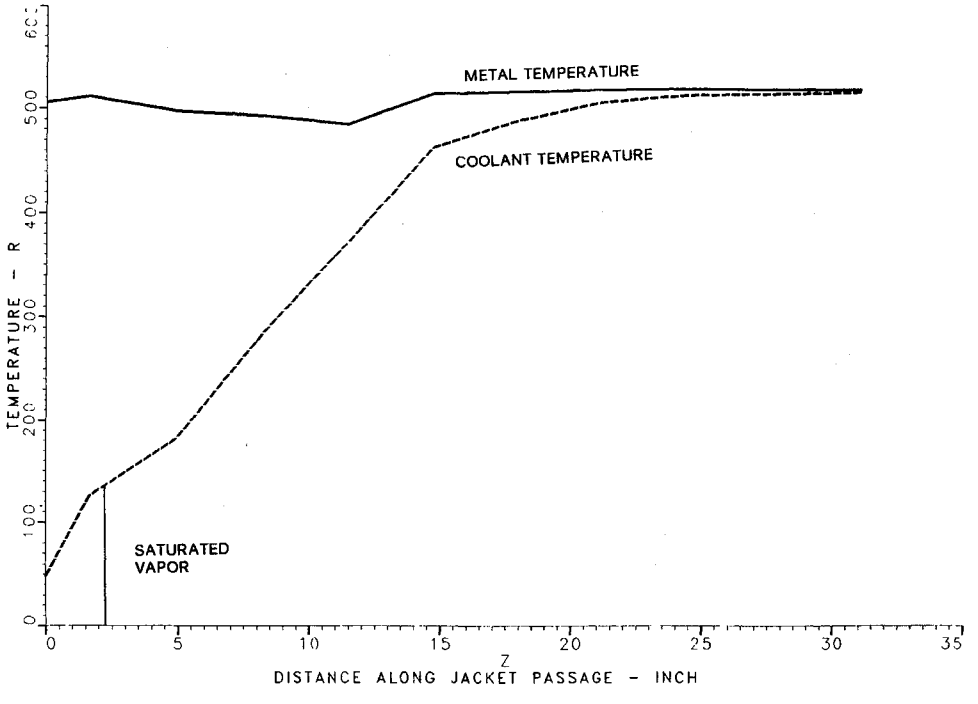

Fig. 8 Nozzle jacket passage temperature distribution at 0.25 s for 70-psi fuel inlet pressure and 520°R initial metal temperature.

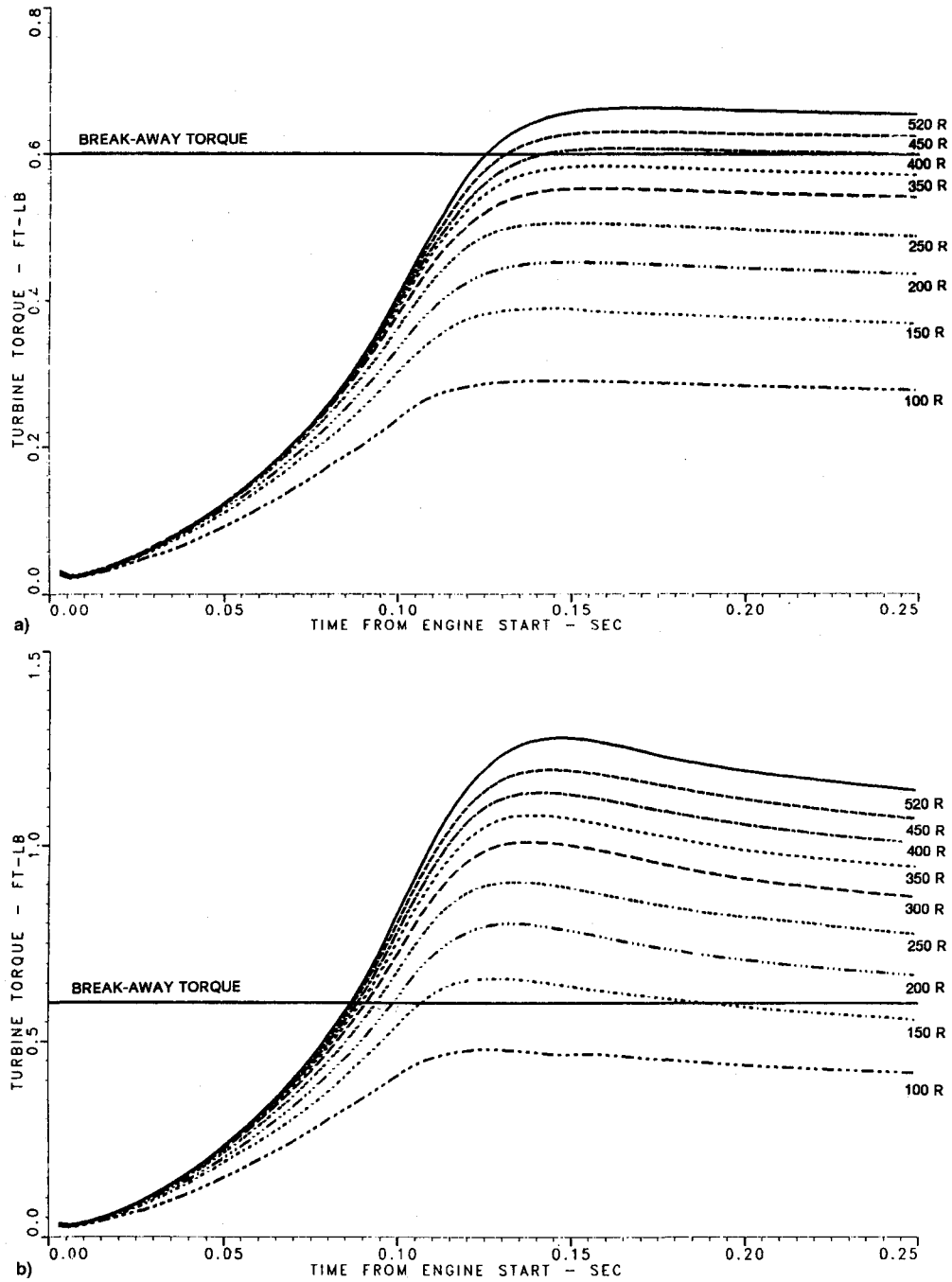

Fig. 9 Turbine torque for various initial temperatures at a) 50- and b) 70-psi fuel inlet pressures.

tained from component performance predictions.[13] Turbine and injector characteristics are summarized in Table 2. Turbine torque vs time from start initiation is shown in Fig. 9 for initial metal temperatures ranging from 520 to 100°R. The predicted torque requirement of 0.6 ft-lb is shown for comparison. Available torque increases from zero and peaks just after jacket inlet conditions reach steady state. Steady-state torque increases with increasing initial jacket metal temperatures. Note that in both Figs. 9a and 9b, corresponding to 70- and 50-psi inlet pressures, respectively, there are a number of initial jacket metal temperature conditions in which turbopump rotation will not occur, i.e., 0.6 ft-lb of torque will not be generated.

VI. Summary and Conclusions

An analytical technique is presented to predict the dynamic character of start processes in the fuel system of a liquid hydrogen-fueled rocket engine. The heat transfer and fluid flow rate, phase change, and expansion characteristics have been determined and the resulting available engine turbine torque calculated. The outstanding feature of this model is the accurate representation of fluid thermodynamic properties during phase change and subsequent affects on heat transfer and mass flow rates.

The analysis has determined an initial jacket metal temperature requirement for turbine breakaway for starting an engine with 70- and 50-psi inlet pressures and sea level discharge conditions. Care must be taken during engine prestart conditioning to insure the nozzle jacket is not cooled to this level prior to a start. External start assist mechanisms, e.g., bottled helium spin assist, or additional heat sources must be employed to insure the required turbine torque is achieved.

The techniques developed for this analysis can be applied to a number of engine cycle designs. Similar analysis of the Space Shuttle Main Engine starting characteristics has been

performed using engine data for verification of prediction accuracy.[5] Calculated nozzle jacket heat addition and pressure drop show good agreement with engine data when measured jacket inlet conditions and metal temperatures are used as the analysis boundary conditions. The techniques presented can also be used for predicting cooldown requirements of cryogenic systems, where accurate predictions of nucleate boiling heat transfer are critical. Although this study assumed sea level conditions, high altitude starts can also be simulated, providing appropriate modifications are made to the heat transfer correlations to compensate for low and/or high gravity effects. Since three critical factors vary during space operation, hydrogen tank supply pressure, engine discharge pressure, and the extreme range of nozzle jacket temperatures, analyses of this type are essential to ensure a successful engine start. More accurate predictions at starting capability, including thrust buildup characteristics, could be attained by including oxidizer system and combustion process models in the analysis and by considering other fuel system effects.

References

[1]Sutton, G. P., *Rocket Propulsion Elements—An Introduction to the Engineering of Rockets*, Wiley, New York, 1986.

[2]Carton, D. S., Maxwell, W. R., and Hurden, D., *Rocket Propulsion Technology*, Plenum, New York, 1961.

[3]Kalin, V. M., and Sherstiannikov, V. A., "Hydrodynamic Modeling of the Starting Process in Liquid Propellant Engines," *Acta Astronautica*, Vol. 8, 1979, pp. 231–242.

[4]Huzel, D. K., and Huang, D. H., *Design of Liquid Propellant Rocket Engines*, NASA SP-125, Washington, DC, 1967.

[5]Avampato, T. J., "Dynamic Modeling of Liquid Propellant Rocket Engine Fuel System Start-Up Processes," M.S. Thesis, Univ. of Florida, Gainesville, FL, 1993.

[6]Shapiro, A. H., *The Dynamics and Thermodynamics of Compressible Flow*, Wiley, New York, 1953.

[7]Chen, J. C., "Correlation for Boiling Heat Transfer to Saturated Fluids in Convective Flows," *I&EC Process Design and Development*, Vol. 5, No. 3, 1966, pp. 322–329.

[8]Forster, H. K., and Zuber, N., "Dynamics of Vapor Bubbles and Boiling Heat Transfer," *American Institute of Chemical Engineers*, Vol. 1, No. 4, 1955, pp. 531–535.

[9]Katto, Y., "Prediction of Critical Heat Flux of Subcooled Flow Boiling in Round Tubes," *International Journal of Heat and Mass Transfer*, Vol. 33, No. 9, 1987, pp. 1921–1928.

[10]Hendricks, R. C., Graham, R. W., Hsu, Y. Y., and Friedman, R., "Experimental Heat Transfer Results for Cryogenic Hydrogen Flowing in Tubes Flowing at Subcritical and Supercritical Pressures to 800 Pounds per Square Inch Absolute," NASA TN D-3095, Cleveland, OH, 1965.

[11]Hendricks, R. C., Simoneau, R. J., and Friedman, R., "Heat Transfer Characteristics of Cryogenic Hydrogen from 1000 to 2500 psia Flowing Upward in Uniformly Heated Straight Tubes," NASA TN D-2977, Cleveland, OH, 1966.

[12]Atkinson, K. E., *An Introduction to Numerical Analysis*, Wiley, New York, 1978.

[13]Fredmonski, A. J., and Kubinski, C. A., "Aerodynamic Design of the AETB Oxidizer Turbine," United Technologies, Pratt & Whitney Government Engine Business, Internal Correspondence, West Palm Beach, FL, 1992.